<u>Supplementary Material for "North American Climate in CMIP5 Experiments: Part III: Assessment of 21st Century Projections" by Maloney et al.</u>

As mentioned in the main text, for some analyses, the number of models used was significantly lower than that of the core set, or the RCP4.5 scenario was used rather than RCP8.5. In these cases, while the results are still potentially enlightening, we have placed the details of these analyses into this supplement section. These analyses moisture transport, frost days, East Coast cyclone intensity, and diurnal temperature range changes, as well as an analysis of tropical cyclone activity change using a downscaling technique with a high-resolution model. Also provided in this supplement is a partitioning of projected RCP8.5 temperature and precipitation changes on a regional detail, including a more refined seasonal and model-by-model breakdown.

a. Moisture fluxes

Model projected differences in vertically integrated moisture transport (MT) to 500 hPa (vectors) and its divergence (contours) are shown in Figure S2 for five coupled models, for RCP8.5 (2081-2100) minus historical (1981-2000) experiments. The MT is well simulated in these models in historical simulations (Sheffield et al. 2013a). While the number of models is too few to provide robust conclusions regarding changes in MT, this analysis provides process level support for model agreement/disagreement in precipitation projections. In summer, the models suggest an increased transport in both (East coast and Great Plains) branches of moisture flow, with a poleward intensification in the coastal branch associated with a poleward shift in moisture convergence on the northwest flank of the Atlantic subtropical anticyclone and increased moisture divergence to the south. The increased Great Plains flux is consistent with projected strengthening of the Great Plains low-level jet, as described in more detail below. Three of the five models show increased divergence in the northern plains during summer, and all show increased divergence in the Pacific Northwest that is associated with stronger descending flow in the North Pacific anticyclone, and where model agreement exists on precipitation decrease (Figure 2).

In winter, the models indicate stronger MT from the Pacific into the Northwest, but the latitude of the increased westerly transport is critical in determining whether much of California is in a region of increased or decreased divergence. Agreement does exist that increased southerly MT in the Atlantic sector is the source for stronger convergence in the poleward shifted North Atlantic storm track, while the Gulf coast and Florida would see increased divergence of moisture.

b. Frost days

Figure S3 shows the change in the number of frost days (FDs) simulated by 14 core models between 1979-2005 and 2071-2100. MEM changes of over 40 days occur in the western third of NA from the US western mountains north through the Canadian Rockies to Alaska, and between 20 to 30 days over the eastern two thirds of NA, with less change in the southern U.S.. Most uncertainty exists among the model projections for the West, with multimodel standard deviations of up to 8 days. The highest agreement is in the Canadian Northern Territories. Some of the differences among models can be explained by the historical biases in the models (Sheffield et al., 2013a), which may limit or enhance future changes even if the projected shift in temperature is the same across models. For example, CCSM4 has historically too few FDs in the central US, and projects less of a decrease in this region in the future. The IPSL-CM5A-LR and CSIRO-MK3-6-0 models project the largest decreases in FDs over the western U.S., but these two models also have the largest over-estimation of historic FDs in this region. These results indicate that bias correction of the modeled extreme values of this type can help reduce the uncertainty in future projections.

c. Diurnal temperature range

One robust global climate change signal over the 20th Century was the widespread decline of diurnal temperature range (DTR, T_{max}-T_{min}), especially in winter, resulting from nighttime temperatures warming faster than daytime (Karl et al. 1993, Dai et al 1999, Easterling et al 1997, and Vose et al 2005). Global T_{min} increased by 0.20 °C dec^{-1} while T_{max} raised 0.14 °C dec^{-1} from 1950–2004, resulting in a DTR decrease of 0.07°C (Vose et al., 2005). During the same period over North America, summer T_{max} and T_{min} increased 0.07 and 0.12 °C, respectively, resulting in a -0.05 °C decrease in DTR. A similar decrease (-0.06 °C) occurred in winter. In RCP4.5, the core CMIP5 models of Table 1 project sharp decreases in wintertime DTR in the mid 21st Century, most prominent in an east-west oriented band at northern latitudes where DTR decreases by more than 0.2 ^{o}C/decade (Figure S4). This decrease in DTR is largely due to preferential increases in nighttime temperature. In the southern U.S. and Mexico, DTR is projected to increase, although with larger uncertainty as indicated by the larger inter-model variance. During summer, DTR is projected to slightly increase (<0.15 ^{o}C/decade) in the north central section of the U.S. In the southwestern U.S., the MEM DTR signal is rather weak, which is also accompanied by larger variance among the models, likely due to different treatments of local convection over complex terrain in each model. The uncertainty in projected DTR trend is generally higher in the lower latitudes. If we view the signal (DTR trend) to noise (inter-model variance) ratio as a simple measure of the confidence in the model projections, the northern Rocky Mountain region has smallest uncertainty in future projections.

It should be noted that the spatial pattern of DTR trend in the first half of the 21st century here is surprisingly similar to that simulated for the second half of 20th century in part 2 of this paper series (Sheffield et al., 2013b). Given that the same group of models largely missed the observed decreasing DTR over a large part of the U.S. in the *historical* experiment, caution should be exercised in interpreting largely positive DTR trends over the U.S. during summer in coming decades.

d. Extratropical cyclone intensity distribution

A gradual reduction in the maximum intensity of cyclones occurs within the dashed box region of Fig. 10a for the three future periods (Fig. S5); however, this reduction is delayed around 990 hPa during the first two 30-year periods. By 2069-2098, a 0.5 to 1.5 (5-10%) reduction in the number of cyclones is projected between the 960 and 1010 hPa pressure bins. In contrast, Colle et al. (2013) showed a 5-10% increase in the number of 960-980 hPa cyclones along the U.S. East coast (not shown), as well as a 20-40% increase in more rapid deepening cyclones in this region.

e) Tropical cyclone-like vortices in the eastern North Pacific and North Atlantic

In the main text we only showed the tropical cyclone-like track density and numbers for 5 models, although we analyzed a total of 14 CMIP5 models. A complete analysis of the global TC activity in these 14 models is given in Camargo (2013). In order to complement the results of the main section with this subset of models, here we show the TC tracks of all 14 models in the historical and the RCP8.5 scenario (for the case of the MPI model, RCP4.5 scenario as well) in Figures S6 and S7. As shown in Figs. S6 and S7, most models have almost no TC activity in the Atlantic and eastern North Pacific basin, even though in some cases they are active in the western North Pacific and southern hemisphere (see Camargo 2013). The five chosen models in our subset are the most active in these two basins, but even in these 5 models the number of models TCs in these two basins are still much lower than the observed number.

f. Tropical cyclone downscaling with a high resolution model

To complement the analysis in Section 6b, we use a dynamical downscaling approach in which a high resolution global atmospheric model (GFDL HIRAM; Zhao et al. 2009; Zhao and Held 2012) is integrated and forced by CMIP3 and CMIP5 coupled model projected SSTs and sea ice concentrations. Recent studies suggest that when forced by the observed SSTs and sea-ice concentrations, a global atmospheric model with a resolution ranging from 50km to 20km can accurately simulate many aspects of hurricane frequency and its variability for the past few decades during which reliable observations are available (e.g., Sugi et al. 2002; McDonald et al. 2005; Yoshimura et al. 2006; Oouchi et al. 2006; Bengtsson et al. 2007; Gualdi et al. 2008; LaRow et al. 2008; Zhao et al. 2009).

We first generate a present-day control simulation by prescribing climatological SSTs and sea-ice concentration (seasonally varying with no interannual variability) using time-averaged (1982-2005) Hadley Center Global Sea Ice and Sea Surface Temperature (HadISST) data (Rayner et al. 2003). For the CMIP3 global warming experiments, we add the SST anomalies (also seasonally varying with no interannual variability) projected by the coupled models to the climatological SSTs and double the CO_2 concentration. For the CMIP5 high-resolution time-slice simulations with prescribed SSTs and sea-ice concentrations, the specifications for both the present-day and the future projection experiments also include interannual variability, and feature future SSTs from two GFDL coupled models (ESM and CM3). The results from downscaling the GFDL CMIP5 projections include changes in both SST anomalies and different specifications for greenhouse-gases and aerosols depending on the pathway used (Held et al 2013). The storm detection and tracking algorithm we use in the analysis is described in Zhao et al. (2009).

The GFDL C180HIRAM simulations with CMIP3 model forcing produce a large inter-model spread (standard deviation of fractional changes ~ 0.35) in the N. Atlantic hurricane frequency response to warming (Figure S8a). For example, the two Hadley Center models produce the largest decrease while the ECHAM5 model generates a modest increase of hurricanes. In contrast, the two GFDL CMIP5 models tend to produce an increase especially in the near decade (2026-2035), and in the CM3 projections for RCP4.5. However, for RCP8.5, both the CM3 and ESM produce insignificant change at the late 21st century.

Zhao and Held (2012) found that most of the inter-model spread in the N. Atlantic hurricane frequency response among the CMIP3 models can be explained by a simple relative SST (RSST) index defined as the tropical Atlantic SST minus tropical mean SST. Under global warming scenarios the SST difference between the MDR and the other tropical ocean basins varies from model to model with implications for hurricane activity (Latif et al. 2007; Swanson 2008; Vecchi et al. 2008; Wang and Lee 2008; Xie et al. 2010). The RCP4.5 projections for both near decades and late 21st century from the CM3 and ESM models show consistent relationship between the N. Atlantic hurricane frequency and the RSST (Figure S9a). However, the results from the two late 21st century runs with RCP8.5 show a marked departure from the regression line associated with the largest reduction (38% for CM3-2090-RCP8.5 and 25% for ESM-2090-RCP8.5) in global mean hurricane frequency. This departure is most likely a result of the larger direct effect of the atmospheric greenhouses-gases concentration (RCP8.5) that can suppress global and regional TC/hurricane frequency and therefore shift the hurricane frequency-RSST regression line downward (Held and Zhao 2011). In general, the CMIP5 downscaling results continue to suggest a large uncertainty in future projections of N. Atlantic hurricane frequency, consistent with the analysis in Section 6a-c.

The GFDL CMIP5 downscaling results tend to produce a reduction in east Pacific hurricanes (Figure S8b, S9b). A negative correlation generally exists between the response of east Pacific and the north Atlantic hurricane frequency. When the fractional changes are plotted against the east Pacific RSST index, we also see a strong correlation between east Pacific hurricane frequency and east Pacific RSST. Again, the departure for the two RCP8.5 models at the late 21st century supports that the global mean reduction due to the direct effect of GHG tends to systematically move the regression line downward.

References

Bengtsson, L., K. Hodges, M. Esch, N. Keenlyside, L. Kornblueh, J.-J. Luo, and T. Yamagata, 2007: How may tropical cyclones change in a warmer climate. *Tellus*, **59A**, 539–561.

Colle, B.A., Z. Zhang, K. Lombardo, P. Liu, E. Chang, and M. Zhang, 2013: Historical Evaluation and Future Prediction of Eastern North American and Western Atlantic Extratropical Cyclones in the CMIP5 Models during the Cool Season. *J. Climate*, **26**, 6882–6903.

Camargo, S.J., 2013. Global and regional aspects of tropical cyclone activity in the CMIP5 models. J. Climate, in press, doi: 10.1175/JCLI-D-12-00549.1.

Dai, A., K. E. Trenberth, and T. R. Karl, 1999: Effects of Clouds, Soil Moisture, Precipitation, and Water Vapor on Diurnal Temperature Range. J. Climate, 12, 2451–2473, doi: 10.1175/1520-0442(1999)0122.0.CO;2.

Easterling, D.R., B. Horton, P. D. Jones, T. C. Peterson, T. R. Karl, D. E. Parker, M. J. Salinger, V. Razuvayev, N. Plummer, P. Jamason and C. K. Folland, 1997: Maximum and Minimum Temperature Trends for the Globe. *Science*, **277**, 364-367. DOI: 10.1126/science.277.5324.364.

Gualdi, S., E. Scoccimarro, and A. Navarra, 2008: Changes in tropical cyclone activity due to global warming: results from a high-resolution coupled general circulation model. *J. Climate*, **21**, 5204–5228.

Held, I. M. and coauthors, 2013: High resolution AMIP simulation for CMIP5 using GFDL's HIRAM model. *J. Climate*, manuscript in preparation.

Held, I. and M. Zhao, 2011: The response of tropical cyclone statistics to an increase in CO2 with fixed sea surface temperatures. *J. Climate*, **24**, 5353–5364.

Karl, T. R., and Coauthors, 1993: A New Perspective on Recent Global Warming: Asymmetric Trends of Daily Maximum and Minimum Temperature. *Bull. Amer. Meteor. Soc.*, **74**, 1007–1023.

Latif, M., N. Keenlyside, and J. Bader, 2007: Tropical sea surface temperature, vertical wind shear, and hurricane development. *Geophys. Res. Lett*., **34**, doi:10.1029/2006GL027969.

LaRow, T., Y.-K. Lim, D. Shin, E. Chassignet, and S. Cocke, 2008: Atlantic basin seasonal hurricane simulations. *J. Climate*, **21**, 3191–3206.

McDonald, R., D. Bleaken, D. Creswell, V. Pope, and C. Senior, 2005: Tropical storms: representation and diagnosis in climate models and the impact of climate change. *Clim. Dyn*., **25**, 19–36.

Oouchi, K., J. Yoshimura, H. Yoshimura, R. Mizuta, S. Kusunoki, and A. Noda, 2006: Tropical cyclone climatology in a global-warming climate as simulated in a 20 km mesh global atmospheric model: Frequency and wind intensity analysis. *J. Meteor. Soc. Japan*, **84**, 259–276.

Rayner, R., D. Parker, E. Horton, C. Folland, L. Alexander, and D. Rowel, 2003: Global analyses of sea surface temperature, sea ice, and night marine air temperature since the late nineteenth century. *J. Geophys. Res*., **108**, D14,4407,doi:10.1029/2002JD002670.

Sheffield, J., and others, 2013a: North American Climate in CMIP5 Experiments. Part I: Evaluation of 20th Century Continental and Regional Climatology. *J. Climate*, **26**, 9209–9245.

Sheffield, J., and others, 2013b: North American Climate in CMIP5 Experiments. Part II: Evaluation of 20th Century Intra-seasonal to Decadal Variability. *J. Climate*, **26**, 9247–9290.

Swanson, K. L., 2008: Nonlocality of Atlantic tropical cyclone intensities. *Geochem. Geophys. Geosyst*., **9**, Q04V01. doi:10.1029/2007GC001844.

Sugi, M., A. Noda, and N. Sato, 2002: Influence of the global warming 105 on tropical cyclone climatology: An experiment with the JMA global model. *J. Meteor. Soc. Japan*, **80**, 249–272.

Vecchi, G. A., K. Swanson, and B. Soden, 2008: Whither hurricane activity? *Science*, **322**, 687-689.

Vose, R. S., D. R. Easterling, and B. Gleason (2005), Maximum and minimum temperature trends for the globe: An update through 2004, *Geophys. Res. Lett*., **32**, L23822, doi:10.1029/2005GL024379.

Wang, C., and S.-K. Lee, 2008: Global warming and United States landfalling hurricanes. *Geophys. Res. Lett*., **35**, L02708. doi:10.1029/2007GL032396.

Xie, S.-P., C. Deser, G.A. Vecchi, J. Ma, H. Teng, and A.T. Wittenberg, 2010: Global warming pattern formation: Sea surface temperature and rainfall. *J. Climate*, **23**, 966–986.

Yoshimura, J., M. Sugi, and A. Noda, 2006: Influence of greenhouse warming on tropical cyclone frequency. *J. Meteor. Soc. Japan*, **84**, 405–428.

Zhao, M., and I. M. Held, 2012: TC-Permitting GCM Simulations of Hurricane Frequency Response to Sea Surface Temperature Anomalies Projected for the Late-Twenty-First Century. *J. Climate*, **25**, 2995–3009.

Zhao, M., I. M. Held, S.-J. Lin, and G. A. Vecchi, 2009: Simulations of global hurricane climatology, interannual variability, and response to global warming using a 50km resolution GCM. *J. Climate*, **22**, 6653–6678.

Table S1: RCP8.5, near surface air temperature change (2070 to 2099) - (1961 to 1990): Annual mean. Regions are defined in Figure 4, except conUS, which represents the lower 48 U.S. states.

Model Name	NA	conUS	ALA	NEC	ENA	CNA	WNA	CAM
bcc-csm1-1	5.7	4.8	7.4	7.1	4.9	4.9	5.4	3.5
CanESM2	7.1	6.0	8.9	9.0	6.3	6.0	6.6	5.3
CCSM4	5.4	4.7	7.0	6.3	4.8	4.9	4.9	3.9
CNRM-CM5	5.4	4.8	6.8	6.6	4.7	4.8	5.2	3.5
CSIRO-Mk3-6-0	5.8	5.5	6.7	6.3	5.1	5.8	5.8	4.9
GFDL-CM3	7.7	6.3	10.0	11.2	7.1	6.3	6.3	5.3
GFDL-ESM2M	4.0	3.8	4.3	4.7	4.0	3.8	3.6	3.5
GISS-E2-R	3.9	3.6	4.7	4.7	3.9	3.7	3.4	3.3
HadGEM2-ES	7.8	6.6	10.1	10.2	7.3	7.0	6.7	5.2
inmcm4	4.1	3.7	5.0	5.0	3.5	3.8	3.9	3.2
IPSL-CM5A-LR	6.5	6.1	7.5	7.5	5.8	6.1	6.4	5.6
MIROC5	6.8	5.6	8.5	9.9	6.0	6.2	5.6	4.2
MIROC-ESM	7.6	6.8	9.1	9.7	7.2	7.3	7.1	4.8
MPI-ESM-LR	5.8	5.0	7.7	6.9	5.1	5.2	5.2	4.6
MRI-CGCM3	4.0	3.3	4.7	5.2	3.7	3.3	3.4	3.3
NorESM1-M	5.8	5.1	7.4	7.5	5.3	5.5	5.2	4.0
MM	**5.8**	**5.1**	**7.2**	**7.4**	**5.3**	**5.3**	**5.3**	**4.3**
std	**1.4**	**1.1**	**1.8**	**2.1**	**1.2**	**1.2**	**1.2**	**0.8**

Table S2: RCP8.5, near surface air temperature change (2070 to 2099) - (1961 to 1990): DJF mean. Regions are defined in Figure 4, except conUS, which represents the lower 48 U.S. states.

Model Name	NA	conUS	ALA	NEC	ENA	CNA	WNA	CAM
bcc-csm1-1	7.6	4.7	11.6	12.5	5.4	5.0	6.3	2.7
CanESM2	8.4	5.7	12.8	13.1	6.2	5.7	6.7	5.1
CCSM4	6.4	4.7	9.5	9.3	5.0	5.0	5.1	3.7
CNRM-CM5	7.3	5.7	10.6	10.7	6.0	6.0	6.1	3.5
CSIRO-Mk3-6-0	7.0	5.3	9.7	9.6	5.4	6.2	5.8	4.5
GFDL-CM3	8.3	4.8	13.7	14.7	6.5	4.8	5.2	4.3
GFDL-ESM2M	4.7	3.4	7.1	7.0	4.0	3.6	3.4	3.0
GISS-E2-R	4.0	3.0	6.0	5.6	4.2	3.1	2.6	2.9
HadGEM2-ES	9.5	6.9	14.2	14.6	7.8	8.0	6.9	5.0
inmcm4	5.3	3.9	7.4	8.0	4.6	4.1	4.5	2.2
IPSL-CM5A-LR	7.1	5.9	9.2	9.8	5.8	6.1	6.4	4.7
MIROC5	8.1	5.4	12.2	13.9	6.4	6.1	5.6	3.8
MIROC-ESM	8.8	6.7	12.3	12.6	7.8	7.3	7.5	4.3
MPI-ESM-LR	7.0	4.4	11.6	10.4	4.9	4.7	5.3	4.2
MRI-CGCM3	4.8	3.2	6.4	8.1	4.3	3.2	3.4	3.0
NorESM1-M	6.4	5.0	7.9	10.4	5.8	5.5	4.6	3.8
MM	**6.9**	**4.9**	**10.1**	**10.6**	**5.6**	**5.3**	**5.4**	**3.8**
std	**1.6**	**1.2**	**2.6**	**2.7**	**1.2**	**1.4**	**1.4**	**0.9**

Table S3: RCP8.5, near-surface air temperature change (2070 to 2099) - (1961 to 1990): MAM mean. Regions are defined in Figure 4, except conUS, which represents the lower 48 U.S. states.

Model Name	NA	conUS	ALA	NEC	ENA	CNA	WNA	CAM
bcc-csm1-1	4.5	4.1	5.4	5.0	4.2	4.0	4.2	3.9
CanESM2	6.3	5.8	6.9	7.7	5.7	5.7	5.9	5.4
CCSM4	4.7	4.3	5.7	5.2	4.5	4.5	4.2	4.1
CNRM-CM5	4.5	4.0	5.9	5.0	3.7	3.5	4.5	3.7
CSIRO-Mk3-6-0	4.8	4.9	5.3	4.3	4.9	5.1	4.5	5.1
GFDL-CM3	7.2	5.6	9.2	10.8	6.7	5.5	5.7	5.2
GFDL-ESM2M	3.8	3.5	4.2	4.3	3.5	3.2	3.6	3.7
GISS-E2-R	3.7	3.7	4.2	3.9	3.8	3.8	3.2	3.5
HadGEM2-ES	7.3	5.4	11.2	10.3	6.1	5.2	5.6	5.2
inmcm4	4.1	3.2	5.2	5.5	3.8	3.2	3.2	3.8
IPSL-CM5A-LR	5.6	5.3	7.1	5.3	4.8	5.2	5.6	5.5
MIROC5	6.8	6.3	7.3	9.3	7.0	7.1	5.9	4.3
MIROC-ESM	7.8	6.9	8.8	10.1	7.8	7.3	7.2	5.1
MPI-ESM-LR	5.5	4.4	7.8	6.7	4.5	4.4	4.8	4.6
MRI-CGCM3	3.2	2.8	3.7	3.8	3.0	2.5	2.6	3.6
NorESM1-M	5.3	4.8	6.7	6.5	4.8	5.1	4.8	4.3
MM	**5.3**	**4.7**	**6.5**	**6.5**	**4.9**	**4.7**	**4.7**	**4.4**
std	**1.4**	**1.1**	**2.0**	**2.4**	**1.4**	**1.3**	**1.2**	**0.7**

Table S4: RCP8.5, near surface air temperature change (2070 to 2099) - (1961 to 1990): JJA mean. Regions are defined in Figure 4, except conUS, which represents the lower 48 U.S. states.

Model Name	NA	conUS	ALA	NEC	ENA	CNA	WNA	CAM
bcc-csm1-1	4.8	5.3	4.6	4.2	5.1	5.2	5.6	4.0
CanESM2	7.0	6.5	7.4	7.9	7.0	6.4	7.4	5.4
CCSM4	5.0	5.1	5.5	4.5	5.0	5.1	5.6	3.9
CNRM-CM5	4.6	4.8	4.3	4.7	4.3	4.7	5.2	3.5
CSIRO-Mk3-6-0	5.3	6.3	3.9	4.2	5.5	6.3	6.5	5.2
GFDL-CM3	8.0	7.7	8.3	10.2	8.2	7.7	7.5	6.0
GFDL-ESM2M	3.5	4.2	2.3	3.0	4.1	4.1	3.8	3.9
GISS-E2-R	3.9	4.2	3.6	4.3	3.7	4.0	4.2	3.2
HadGEM2-ES	6.9	7.2	6.2	6.9	7.7	7.4	7.6	5.2
inmcm4	3.2	4.0	2.1	2.5	2.7	3.8	4.1	3.7
IPSL-CM5A-LR	6.6	6.8	6.2	7.0	6.1	6.7	7.0	6.3
MIROC5	5.9	5.4	6.1	7.4	5.2	6.1	5.5	4.6
MIROC-ESM	7.0	7.1	7.3	7.7	6.5	7.7	7.2	5.3
MPI-ESM-LR	5.2	5.7	4.3	5.2	5.7	5.8	5.3	4.7
MRI-CGCM3	3.4	3.8	2.5	3.3	3.6	3.8	3.7	3.6
NorESM1-M	5.7	5.3	6.7	5.9	5.3	5.7	5.9	4.0
MM	**5.4**	**5.6**	**5.1**	**5.6**	**5.4**	**5.7**	**5.8**	**4.5**
std	**1.5**	**1.2**	**1.9**	**2.1**	**1.5**	**1.3**	**1.3**	**0.9**

Table S5: RCP8.5, near-surface air temperature change (2070 to 2099) - (1961 to 1990): SON mean. Regions are defined in Figure 4, except conUS, which represents the lower 48 U.S. states.

Model Name	NA	conUS	ALA	NEC	ENA	CNA	WNA	CAM
bcc-csm1-1	5.8	5.1	8.0	6.7	5.1	5.4	5.4	3.6
CanESM2	6.6	6.0	8.4	7.2	6.2	6.1	6.3	5.3
CCSM4	5.3	4.7	7.3	6.2	4.8	5.0	4.8	3.8
CNRM-CM5	5.1	4.7	6.6	5.9	4.8	4.9	4.9	3.5
CSIRO-Mk3-6-0	6.2	5.7	8.0	6.8	4.7	5.7	6.3	4.9
GFDL-CM3	7.4	6.9	9.0	9.2	7.1	7.0	6.5	5.7
GFDL-ESM2M	3.9	4.2	3.7	4.4	4.3	4.4	3.7	3.4
GISS-E2-R	4.0	3.7	5.0	4.9	3.8	3.8	3.4	3.5
HadGEM2-ES	7.5	7.1	8.7	8.9	7.7	7.4	6.8	5.3
inmcm4	3.9	3.7	5.2	4.2	2.8	3.9	3.9	2.9
IPSL-CM5A-LR	6.8	6.5	7.6	7.8	6.5	6.5	6.5	5.7
MIROC5	6.3	5.4	8.5	8.8	5.6	5.7	5.3	4.0
MIROC-ESM	6.8	6.6	7.9	8.2	6.8	7.1	6.3	4.5
MPI-ESM-LR	5.6	5.6	7.0	5.5	5.3	5.7	5.4	4.8
MRI-CGCM3	4.4	3.6	6.2	5.8	3.7	3.5	3.9	3.1
NorESM1-M	6.0	5.3	8.3	7.3	5.1	5.7	5.3	4.0
MM	**5.7**	**5.3**	**7.2**	**6.7**	**5.3**	**5.5**	**5.3**	**4.2**
std	**1.2**	**1.1**	**1.5**	**1.6**	**1.3**	**1.2**	**1.1**	**0.9**

Table S6: RCP8.5, % precipitation change (2070 to 2099) - (1961 to 1990): Annual mean. Regions are defined in Figure 4, except conUS, which represents the lower 48 U.S. states.

Model Name	NA	conUS	ALA	NEC	ENA	CNA	WNA	CAM
CanESM2	15.9	12.1	41.4	28.7	11.1	7.7	22.6	-17.8
CCSM4	7.2	5.8	25.6	14.7	10.4	8.0	6.9	-18.9
CNRM-CM5	11.9	8.9	26.6	22.4	10.3	6.0	13.3	-4.0
CSIRO-Mk3-6-0	8.6	6.7	27.1	18.2	17.0	7.0	5.9	-18.5
GFDL-CM3	17.7	9.0	51.8	32.9	16.8	14.5	11.1	-5.2
GFDL-ESM2M	9.4	2.7	18.4	19.2	8.1	4.8	4.2	6.3
GISS-E2-R	5.1	4.2	15.5	13.9	14.6	9.3	-0.3	-11.5
HadGEM2-ES	10.7	5.2	33.9	26.6	10.0	9.6	2.1	-11.6
inmcm4	4.6	-0.6	24.9	16.7	4.1	1.0	4.9	-27.6
IPSL-CM5A-LR	4.6	-3.5	24.4	19.7	6.1	-6.5	3.5	-38.2
MIROC5	8.0	0.6	23.7	26.3	12.6	-3.0	4.3	-6.7
MIROC-ESM	14.2	2.8	36.4	32.4	7.0	4.4	8.3	1.1
MPI-ESM-LR	10.0	4.8	33.5	23.5	13.7	7.7	4.3	-14.3
MRI-CGCM3	11.7	7.7	28.1	28.1	14.5	8.8	7.5	-4.0
NorESM1-M	6.4	1.6	25.6	20.5	14.0	2.0	5.6	-25.1
MM	**9.7**	**4.5**	**29.1**	**22.9**	**11.4**	**5.4**	**6.9**	**-13.1**
std	**4.0**	**4.1**	**9.1**	**6.1**	**3.9**	**5.3**	**5.5**	**11.7**

Table S7: RCP8.5, % precipitation change (2070 to 2099) - (1961 to 1990): DJF mean. Regions are defined in Figure 4, except conUS, which represents the lower 48 U.S. states.

Model Name	NA	conUS	ALA	NEC	ENA	CNA	WNA	CAM
CanESM2	26.3	22.2	45.1	51.7	24.0	19.4	28.2	-30.4
CCSM4	14.4	14.4	29.3	31.5	18.0	18.2	17.3	-31.7
CNRM-CM5	17.6	15.6	30.3	40.3	17.7	6.8	22.8	-20.6
CSIRO-Mk3-6-0	12.6	3.3	40.6	34.7	9.5	-5.1	17.9	-34.1
GFDL-CM3	27.0	20.1	61.3	60.1	37.9	27.7	14.9	-11.7
GFDL-ESM2M	14.2	8.3	39.7	36.0	14.2	12.2	10.7	-16.9
GISS-E2-R	9.2	10.1	11.9	18.9	31.0	17.2	1.4	-12.9
HadGEM2-ES	25.5	22.4	52.9	66.1	26.2	28.5	11.6	-8.8
inmcm4	8.4	6.5	13.3	22.9	6.0	4.9	18.7	-31.3
IPSL-CM5A-LR	11.3	2.5	24.4	49.7	11.0	-12.2	21.4	-55.3
MIROC5	12.1	3.1	27.5	43.9	16.2	3.4	6.4	-18.2
MIROC-ESM	19.3	3.2	45.8	54.6	13.5	12.3	8.0	-9.5
MPI-ESM-LR	16.3	10.5	50.9	37.8	22.2	11.9	10.1	-26.3
MRI-CGCM3	11.9	13.4	12.8	38.2	21.8	10.1	15.6	-29.7
NorESM1-M	10.4	1.6	28.3	41.8	17.1	13.2	6.0	-33.3
MM	**15.8**	**10.5**	**34.3**	**41.9**	**19.1**	**11.2**	**14.1**	**-24.7**
std	**6.2**	**7.3**	**15.3**	**13.0**	**8.4**	**10.9**	**7.2**	**12.4**

Table S8: RCP8.5, % precipitation change (2070 to 2099) - (1961 to 1990): MAM mean. Regions are defined in Figure 4, except conUS, which represents the lower 48 U.S. states.

Model Name	NA	conUS	ALA	NEC	ENA	CNA	WNA	CAM
CanESM2	19.2	5.8	53.6	46.1	18.6	3.6	20.3	-10.7
CCSM4	7.9	5.9	22.1	17.5	9.6	12.4	4.2	-16.1
CNRM-CM5	13.2	9.2	30.0	27.1	13.7	7.8	13.6	-4.2
CSIRO-Mk3-6-0	16.4	13.4	30.2	23.6	22.0	20.2	5.7	-10.7
GFDL-CM3	23.5	16.1	43.9	53.5	26.0	23.1	19.6	-23.7
GFDL-ESM2M	8.8	7.2	13.4	17.5	13.0	11.1	7.5	-25.7
GISS-E2-R	6.7	7.6	11.5	10.8	18.0	12.7	3.6	-22.1
HadGEM2-ES	17.8	12.8	51.4	36.8	22.7	21.5	4.1	-17.3
inmcm4	10.7	7.9	27.4	24.8	13.3	13.8	8.5	-35.4
IPSL-CM5A-LR	1.5	-2.9	10.4	9.0	8.2	-8.0	0.1	-50.7
MIROC5	14.0	5.9	33.7	33.5	15.6	5.3	13.7	-2.7
MIROC-ESM	20.6	13.1	33.6	41.7	16.9	19.5	14.2	-2.7
MPI-ESM-LR	9.9	6.2	34.9	27.8	16.4	11.2	6.3	-40.4
MRI-CGCM3	14.2	10.0	32.8	44.6	18.0	14.4	9.0	-20.8
NorESM1-M	9.7	7.0	24.6	18.2	18.5	16.9	5.2	-25.1
MM	**12.9**	**8.3**	**30.2**	**28.8**	**16.7**	**12.4**	**9.0**	**-20.5**
std	**5.9**	**4.5**	**13.0**	**13.5**	**4.8**	**8.0**	**6.0**	**13.9**

Table S9: RCP8.5, % precipitation change (2070 to 2099) - (1961 to 1990): JJA mean. Regions are defined in Figure 4, except conUS, which represents the lower 48 U.S. states.

Model Name	NA	conUS	ALA	NEC	ENA	CNA	WNA	CAM
CanESM2	2.7	8.7	26.4	6.2	-1.4	-3.3	17.8	-22.6
CCSM4	-2.2	-3.8	22.3	2.8	6.8	-5.7	-8.9	-24.8
CNRM-CM5	5.9	2.7	24.4	12.3	4.7	1.7	2.8	-6.7
CSIRO-Mk3-6-0	-0.3	2.7	16.0	7.9	17.7	4.7	-13.5	-17.7
GFDL-CM3	9.2	0.8	55.1	12.5	5.4	7.4	4.2	-12.1
GFDL-ESM2M	3.0	-2.0	9.7	9.2	1.8	0.7	-3.2	1.9
GISS-E2-R	-0.1	-4.7	17.1	12.3	0.6	2.5	-9.7	-6.8
HadGEM2-ES	-9.6	-20.2	14.6	3.1	-10.3	-23.9	-19.0	-25.8
inmcm4	0.1	-7.8	32.4	14.2	4.2	-8.3	-10.1	-30.1
IPSL-CM5A-LR	-4.5	-11.3	21.8	2.9	1.2	-10.6	-14.2	-37.8
MIROC5	-2.1	-5.3	11.5	12.3	6.3	-13.8	-6.1	-15.0
MIROC-ESM	3.3	-10.0	29.9	18.8	-3.3	-16.7	-0.9	-11.3
MPI-ESM-LR	0.2	-1.9	18.1	9.2	3.2	2.3	-6.0	-16.2
MRI-CGCM3	10.5	3.3	37.2	23.4	6.2	7.2	2.3	2.5
NorESM1-M	-0.2	-3.0	20.0	9.3	10.4	-12.0	2.7	-26.1
MM	**1.1**	**-3.5**	**23.8**	**10.4**	**3.6**	**-4.5**	**-4.1**	**-16.6**
std	**5.1**	**7.1**	**11.6**	**5.8**	**6.3**	**9.4**	**9.3**	**11.5**

Table S10: RCP8.5, % precipitation change (2070 to 2099) - (1961 to 1990): SON mean. Regions are defined in Figure 4, except conUS, which represents the lower 48 U.S. states.

Model Name	NA	conUS	ALA	NEC	ENA	CNA	WNA	CAM
CanESM2	18.7	11.4	54.7	29.1	2.9	12.6	21.9	-7.4
CCSM4	10.7	8.6	28.5	16.4	9.1	15.3	9.3	-6.9
CNRM-CM5	13.9	9.3	25.4	22.9	7.1	7.6	14.2	5.5
CSIRO-Mk3-6-0	9.3	5.5	32.3	17.3	18.0	1.0	10.1	-16.3
GFDL-CM3	15.6	-0.8	47.1	32.5	1.2	1.0	6.0	12.5
GFDL-ESM2M	13.9	-2.0	23.1	24.8	4.4	-4.3	2.2	28.3
GISS-E2-R	6.9	6.6	19.1	15.2	16.3	9.9	4.7	-10.3
HadGEM2-ES	17.2	4.9	45.5	31.4	5.1	8.5	9.2	11.7
inmcm4	0.1	-13.0	24.0	10.4	-8.2	-14.4	-0.7	-18.6
IPSL-CM5A-LR	11.4	-0.9	36.4	31.0	5.8	6.8	2.2	-21.9
MIROC5	11.9	-0.6	31.9	27.6	14.6	-4.8	4.3	6.3
MIROC-ESM	16.3	5.2	38.4	28.7	2.3	5.2	12.9	14.5
MPI-ESM-LR	17.4	5.4	42.7	30.3	16.5	7.3	4.7	8.2
MRI-CGCM3	10.8	4.0	25.7	20.5	13.2	3.3	2.2	10.1
NorESM1-M	8.0	1.9	30.3	22.7	12.5	1.4	8.1	-18.9
MM	**12.1**	**3.0**	**33.7**	**24.1**	**8.1**	**3.8**	**7.4**	**-0.2**
std	**4.9**	**6.0**	**10.2**	**6.9**	**7.2**	**7.6**	**5.8**	**15.1**

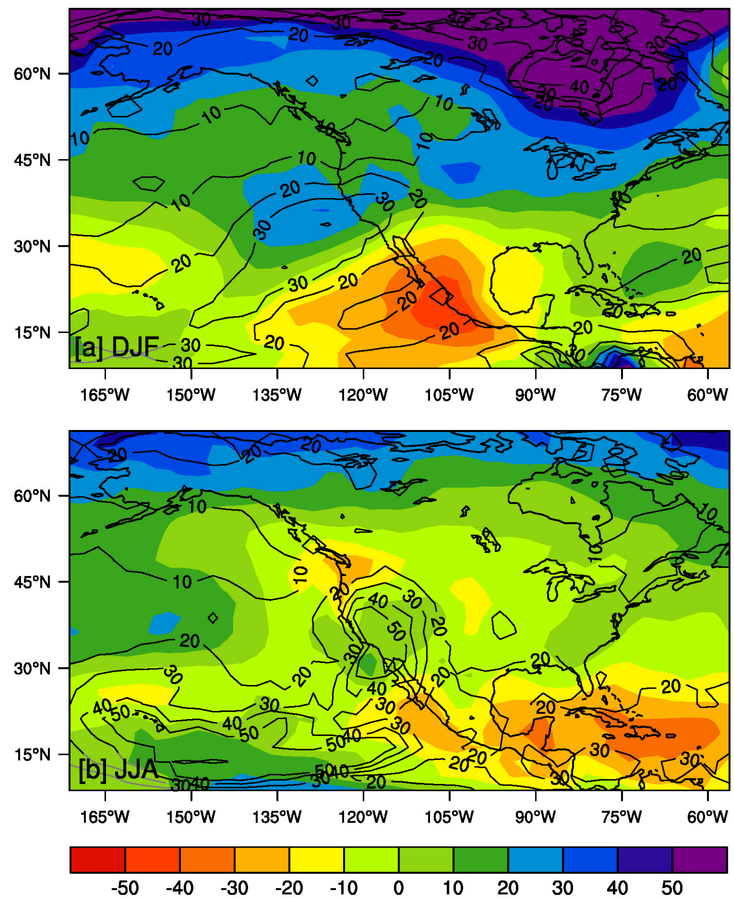

Figure S1. CMIP5 16 member MEM percentage precipitation change (colors) and standard deviation of percent precipitation change (contours) for RCP8.5 for 2070-2099 relative to 1901-1960 base period for December-February (DJF) and June-August (JJA). Models used: BCC-ESM-1, CanESM2, CCSM4, CNRM-CM5, CSIRO-Mk3-6-0, GFDL-CM3, GFDL-ESM2M, GISS-E2-R, HadGEM2-ES, INMCM4, IPSL-CM5A-LR, MIROC5, MIROC-ESM, MPI-ESM-LR, MRI-CGCM3, NORESM1-M.

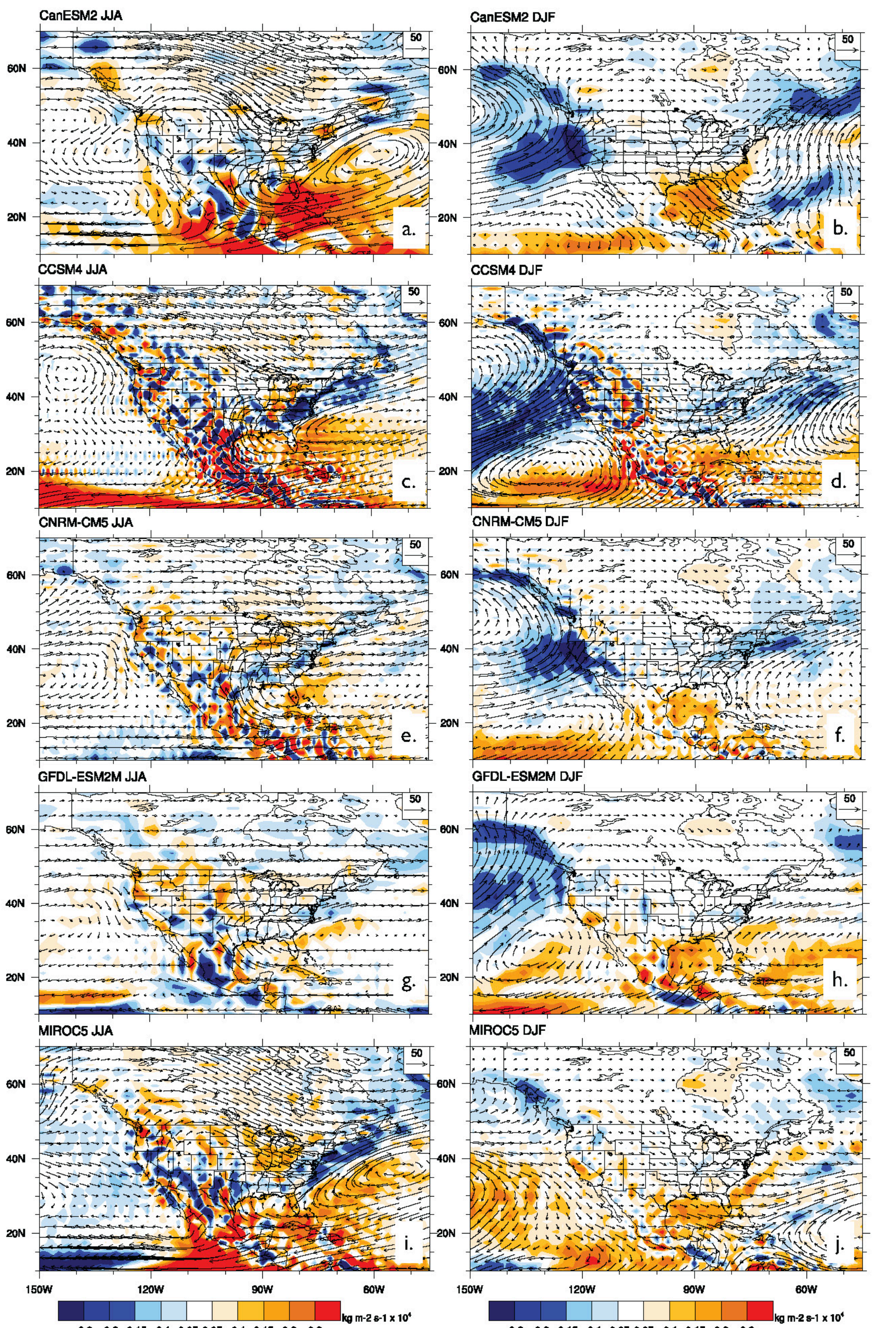

Figure S2. MEM difference in JJA (left) and DJF (right) moisture transport integrated vertically to 500 hPa (VIMT shown as vectors, Kg/ms), and moisture divergence (color contours, $Kg/m^2s \times 10^4$) computed from five coupled models for 2081-2100 from RCP8.5 minus 1981-2000 the historical experiments. The models used are CanESM2, CCSM4, CNRM-CM5, GFDL-ESM2M, and MIROC5, for which one realization of the required 6-hourly fields were available. This figure should be compared with the corresponding analysis from Sheffield et al. 2013a.

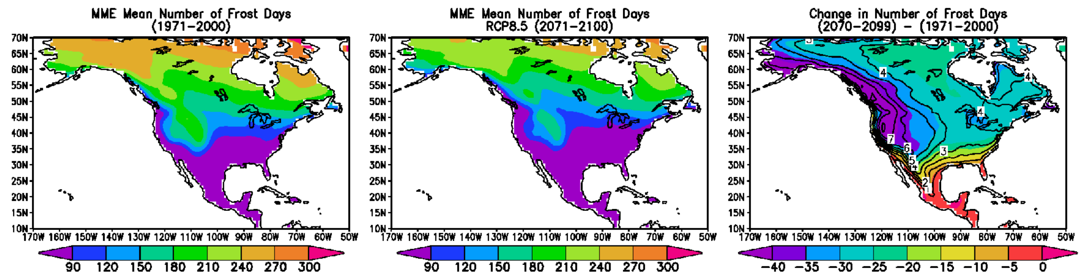

Figure S3. Projected MEM changes in number of frost days (upper right) for 14 core CMIP5 models (BCC-CSM1-1, CanESM2, CCSM4, CSIRO-Mk3-6-0, GFDL-CM3, GFDL-ESM2M, HadGEM2-ES, INMCM4, IPSL-CM5A-LR, MIROC5, MIROC-ESM, MRI-CGCM3, MPI-ESM-LR, NorESM1-M; all single ensemble member r1i1p1) for RCP8.5. Multimodel standard deviations are also plotted in contours. Also shown in the center and left panels are the MEM frost days for the historical runs (1971-2000) and RCP8.5 (2071-2100). Changes are calculated as the difference between the mean for 2071-2100 and 1971-2000. Frost days are calculated as the annual number of days with T_{min} less than $0^{o}C$ (Frick et al., 2002). Values were calculated on the model grid, interpolated to 2.0^{o} resolution and then averaged over 1979-2005 for the "historical" and 2071-2100 for the RCP8.5 scenario.

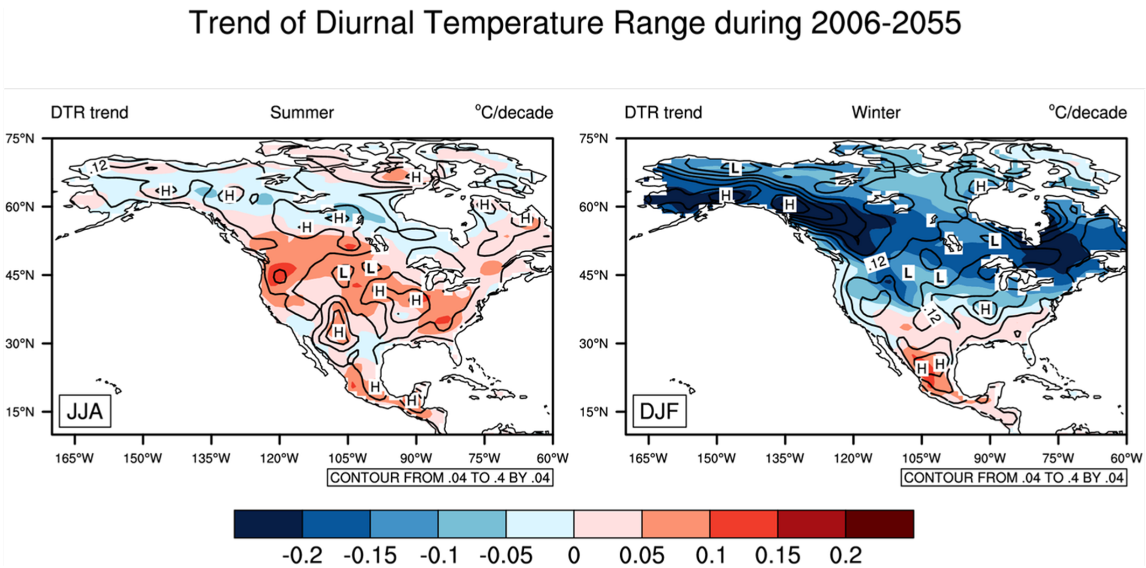

Figure S4. Trend of diurnal temperature range (T_{max} -T_{min}) during 2006-2055 averaged among 16 core models' first member (r1irp1) in the RCP4.5 experiment. The contours are the inter-model standard deviation of the trend.

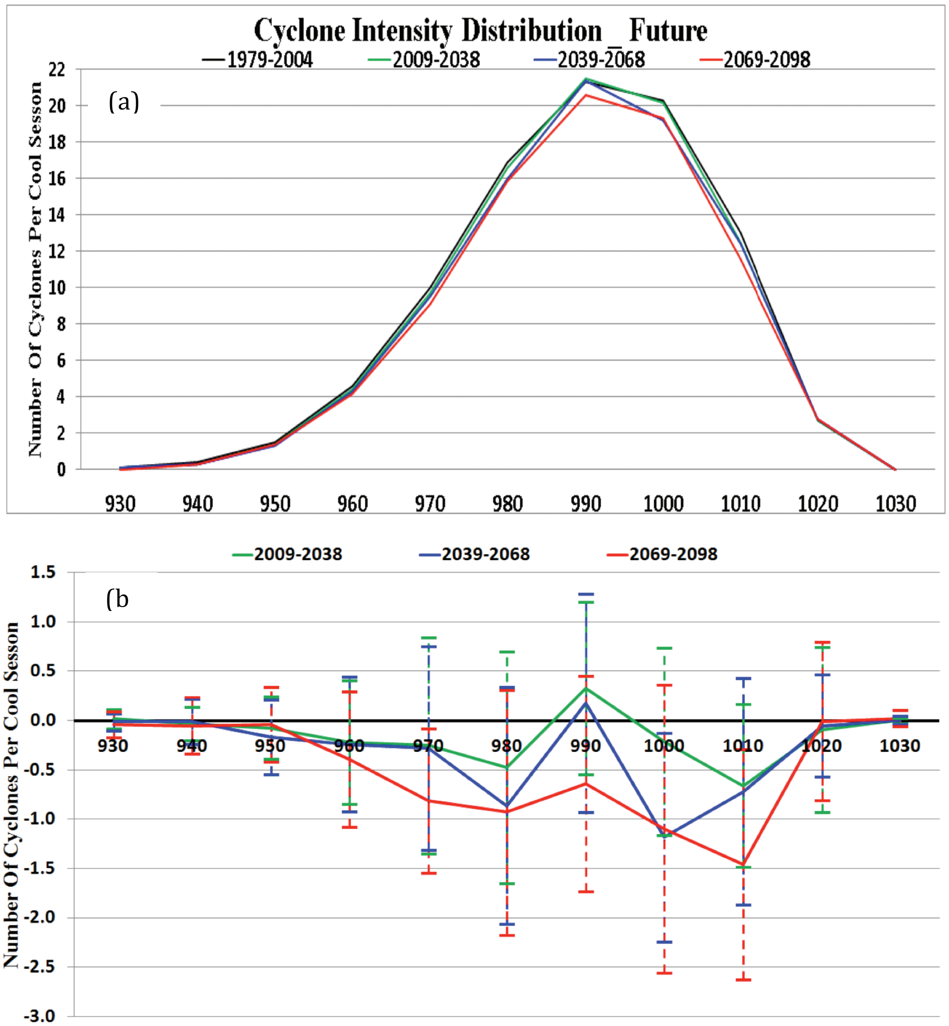

Figure S5. (a) Number of cyclone central pressures at their maximum intensity for the 1979-2004 cool seasons within the dashed box region in Fig. 10a for a 10 hPa range centered every 10 hPa showing the mean historical (black), 2009-2038 (green), 2038-2068 (blue), and 2068-2098 (red) years for 15 CMIP5 models. (b) Same as (a) except the difference and standard deviation between three future periods and the historical 1979-2004 period.

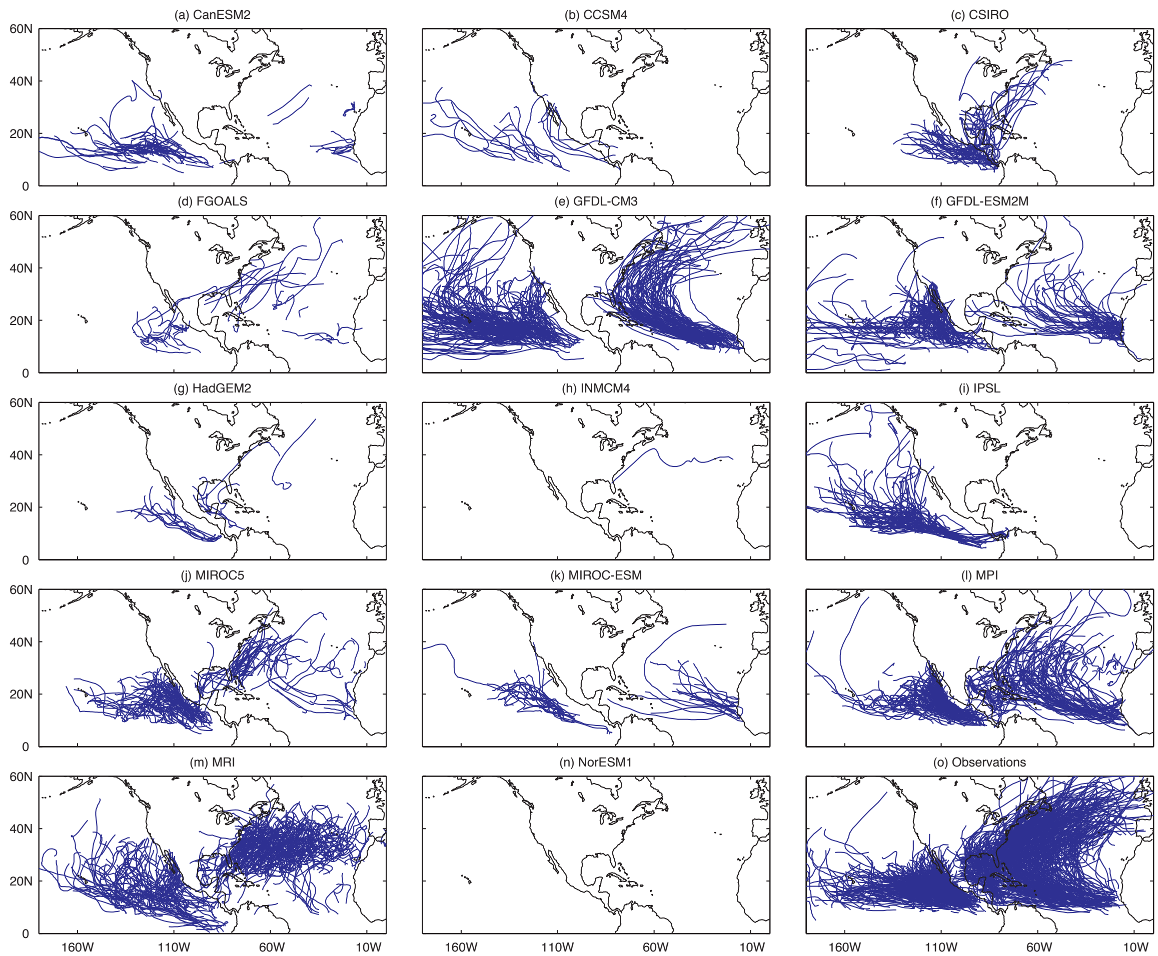

Figure S6: Tracks of model tropical cyclones in 14 CMIP5 core models in the historical runs and in observations in the period 1951-2000 in the eastern north Pacific and north Atlantic basins.

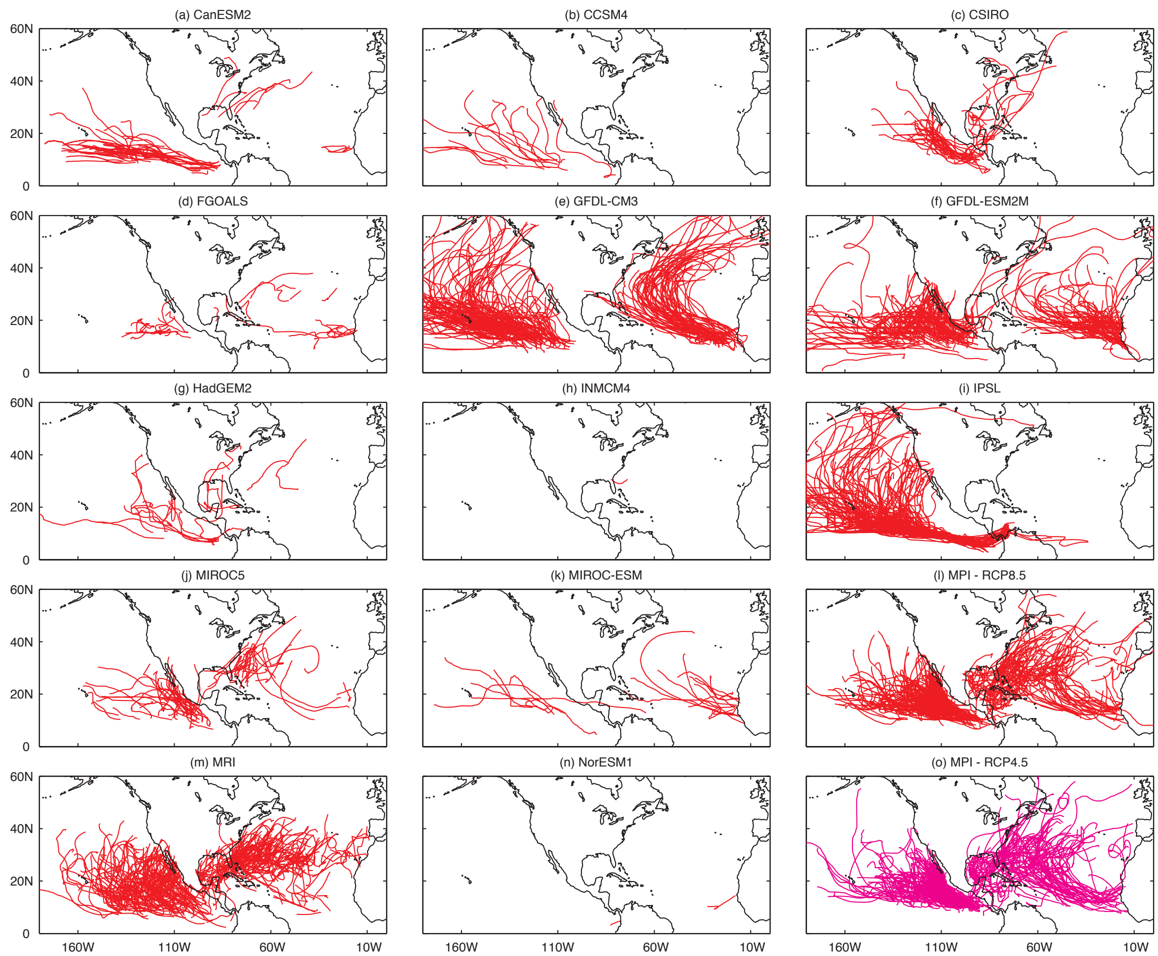

Figure S7: Tracks of model tropical cyclones in 14 core CMIP5 models in the RCP8.5 scenario in the period 2051-2100 in the eastern north Pacific and north Atlantic basins. In the case of the MPI model, the tracks for the RCP4.5 scenario are also shown.

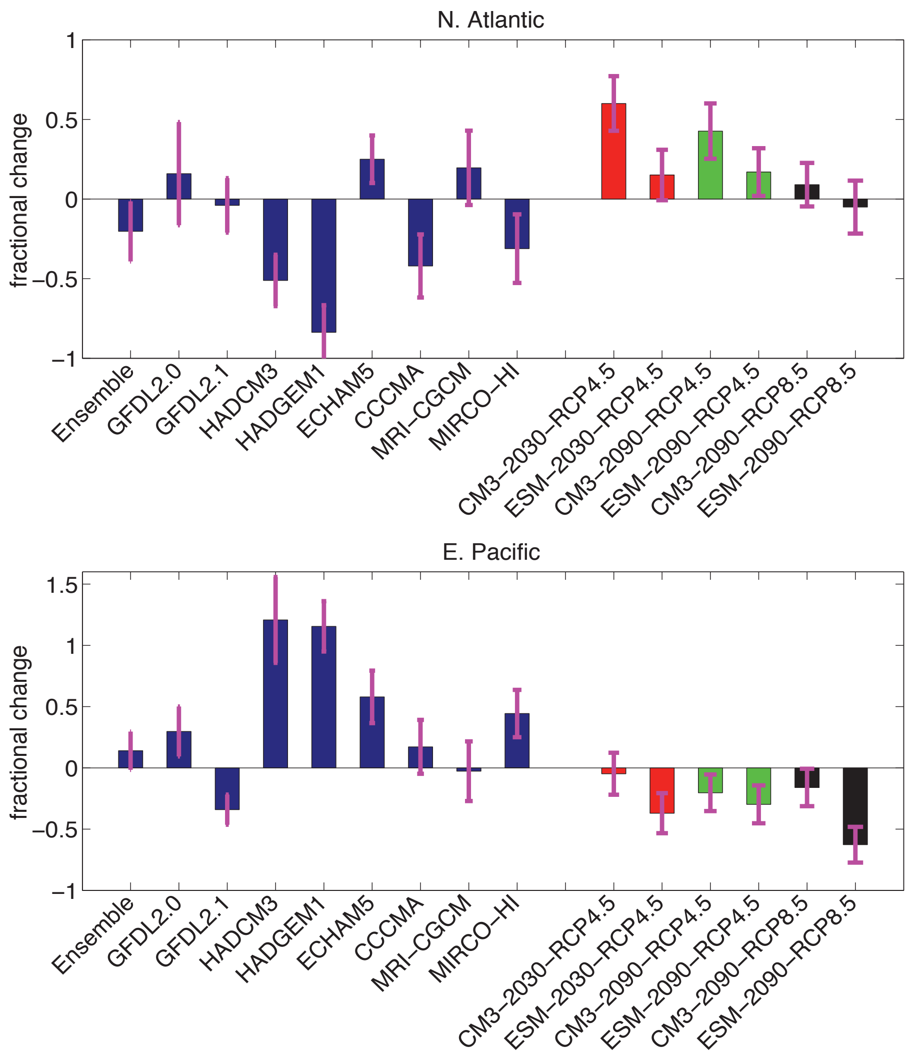

Figure S8. a) Fractional change in N. Atlantic hurricanes frequency downscaled using the GFDL C180HIRAM. Blue bars show results using the CMIP3 models projected SST warming anomalies (and their ensemble mean) at the late 21st century (2080-2100 relative to 2000-2020) for the A1B scenario. The control experiment was integrated for 20 years while most of the warming experiments were carried out for 10 years due to constraints of computer time. Red, green and black bars show results using GFDL CMIP5 model (CM3 and ESM) projected SST warming anomalies (CM3-2030-RCP4.5 and ESM-2030-RCP4.5: 2026-2035 averaged SST anomalies from CM3 and ESM RCP4.5 experiments with radiative gases at RCP4.5 2026-2035 values. CM3-2090-RCP4.5 and ESM-2090-RCP4.5: 2086-2095 averaged SST anomalies from CM3 and ESM RCP4.5 experiments with radiative gases at RCP4.5 2085-2095 values. CM3-2090-RCP8.5 and ESM-2090-RCP8.5: As in CM3-2090-RCP4.5 and ESM-2090-RCP4.5 experiments except using RCP8.5 model projected SST anomalies with radiative gases at RCP8.5 2086-2095 values. The GFDL C180HIRAM present-day experiments contain a 3-member ensemble simulation for the period of 1981 to 2008. The CMIP5 SST anomalies are computed relative to 1981-2008 average. b) As in a) except for the E. Pacific.

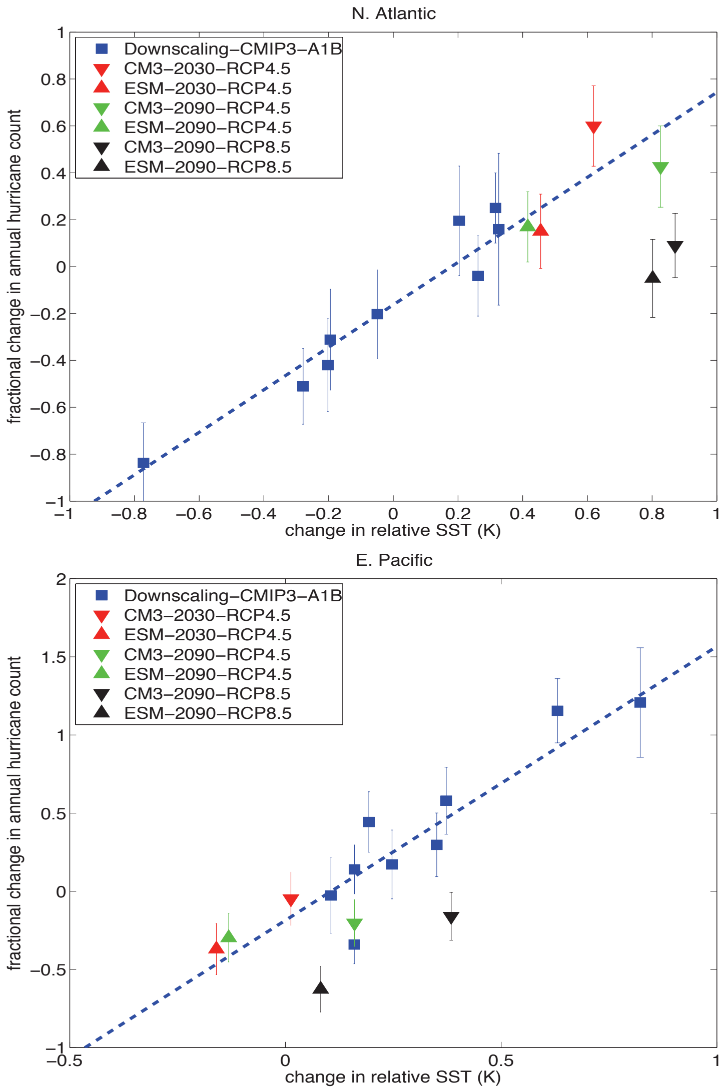

Figure S9. a) the fractional change in N. Atlantic hurricane frequency against changes in a relative SST index defined as the Atlantic Main Development Region (MDR) [80◦W-20◦W, 10◦N-25◦N] SST minus tropical mean [30S-30N] SST in ASO season. b) As in a) except for the E. Pacific, the E. Pacific Main Development Region is defined as [160◦W-100◦W, 7.5◦N-15◦N] .